30

Tonometric Vascular Function Assessment

Jeon Lee[1] and Ki Chang Nam[2]
[1]*Daegu Haany University*
[2]*Korea Electrotechnology Research Institute*
South Korea

1. Introduction

Recently, the number of patients suffered from cardiovascular disease has increased world-widely. Thus, the importance on vascular function assessment has been emphasized and many researchers have tried to develop some non-invasive but effective method for vascular function assessment. If the assessment methods are divided into two, theses are methods based on blood pressure and based on arterial stiffness respectively.

As well known, the cardiovascular risk found to be related to the levels of mean blood pressure (MBP), systolic blood pressure (SBP) and diastolic blood pressure (DBP). And, these three blood pressures were found to be strong determinants of the risks to the brain, heart and kidney. Additionally, in a cross-sectional analysis, the pulse pressure (PP) was shown to be independently related to the degree of cardiac hypertrophy and to be a good predictor of myocardial infarction (MI) (Darne et al., 1989). In the last few years, these parameters of central blood pressure have been verified to more strongly relate to cardiovascular disease than those of brachial blood pressure (Roman et al., 2007).

Meanwhile, arteries store part of the stroke volume during systolic period and drain it during diastolic period. This so called "Windkessel function" thus transforms the pulsatile flow of central arteries into the steady flow required in the peripheral tissues. Under normal condition, approximately 40% of stroke volume is forwarded directly to peripheral tissues during systole and the remainder (60%) is stored in the capacitive arteries. In diastole, the stored blood is squeezed forward into the peripheral circulation (Gerard & Alain, 1999). Increased arterial stiffness causes dysfunction of this function, increasing the incidence of fracture, rupture, and aneurysm formation in arteries and, potentially, the development of atherosclerosis. So, in recent years, great emphasis has been placed on the role of arterial stiffness in the development of cardiovascular diseases.

Even there have been several methods for the assessment of arterial stiffness, two non-invasive methods with PWV (pulse wave velocity) and with AIx (augmentation index) are most widely studied these days. The former is based on the fact that, between two local positions, the pulse wave travels faster for increased arterial stiffness and the latter based on the fact that the reflected pulse wave comes back earlier so to cause the augmentation of systolic pressure. Both PWV and AIx can be calculated by analyzing pulse wave measured with tonometric sensors but, through AIx, the estimation of arterial stiffness has more controversial and challenging issues.

So, in this chapter, the assessment of arterial function with AIx computed from pulse wave measured by tonometric sensors will be dealt. This chapter is composed of brief introduction, outline of arterial tonometry with operation principle, mathematical model and reliable measurement procedure, explanation on arterial stiffness estimation method, introduction of emerging issues arising in this field and conclusion. While we deal with contents mentioned above, we want to share our recent works in between.

2. Arterial tonometry

In the early 1960, applanation tonometry was first implemented by Pressman and Newgard and was shown to be able to measure the pulse wave of a superficial artery non-invasively, so called as 'arterial tonometry' (Pressman & Newgard, 1963). While the sphygmomanometer measures only systolic and diastolic pressure, it provides continuous pulse waveform with pressure sensor placed over a superficial artery. In this section, the operation principle and mathematical model of arterial tonometry are explained to increase the understanding of tonometric measurement.

2.1 Operation principle

The operation principles of arterial tonometry are similar to those of ocular tonometry. But, in arterial tonometry, a rigid structure as like bone is required to support the arterial vessel unlike ocular tonometry. Therefore, the method has been applied mainly to the radial arteries. In Fig. 1, a simplified arterial tonometry principle is shown.

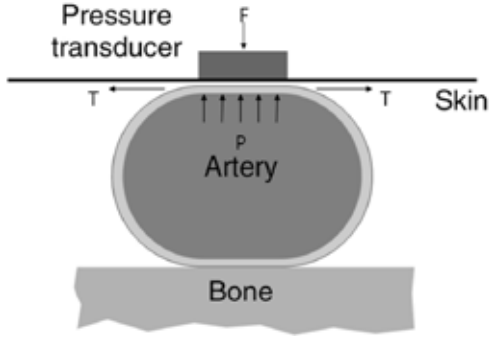

Fig. 1. Arterial tonometry principle

P represents the blood pressure in superficial artery and *F* is the force measured by tonometer transducer. When a pressure transducer is placed over the artery and appropriate pressure is applied so as to partially flatten the artery, the tension vector, *T*, is perpendicular to the pressure vector. Therefore the force, *F*, is independent of *T* and the sensor receives only internal arterial pressure. In practice, to obtain an accurate measurement, several conditions should be satisfied (Eckerle, 2006):

- The artery is supported by rigid structure as like radius.
- The hold-down force flattens a portion of the artery wall, but does not occlude the artery.

- The thickness of the skin over the artery is insignificant, compared to the artery diameter.
- The artery wall behaves essentially like an ideal membrane.
- The artery rider, a force transmission structure to a transducer, is smaller than the flattened area of the artery, and it is centered over the flattened area.
- The spring constant of the force transducer is larger than the effective spring constant of the artery.

2.2 Mathematical model

Deeper insights of arertial tonometry principle can be given by a realistic mathematical model. The first reasonable but simple model for an arterial tonometer was developed by Pressman and Newgard, and consisted of lumped linear elastic elements which represented those the artery, the adjacent tissue, the skin, the tonometer sensor element, and sensor's mounting (Pressman & Newgard, 1963). Although this model provided the relationships among inter-arterial pressure, displacement of sensor frame, and sensor system positioning force, this lumped model was not suitable to analyze remaining problems.

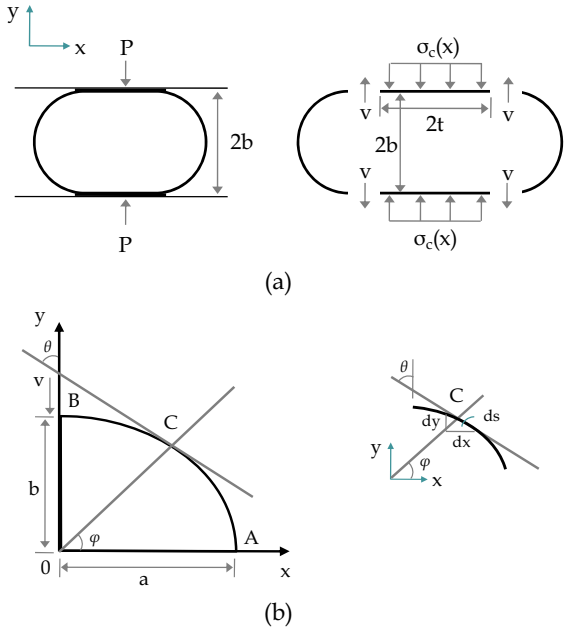

Fig. 2. Cross-sectional continuous model for arterial tonometry. (a) The deflection shape such that the vessel wall consist of free and surface constrained sections. (b) A quadrant of the original cross-section deflected by shear force v=1/2P (Drzewiecki et al., 1983)

So, a mathematical model, which treats the artery and tonometer as solid mechanical structures, was developed and it dealt with the bending and shear deformation neglected in the lumped model (Drzewiecki et al., 1983). In this model shown in Fig. 2, the artery was

regarded as a thin cylindrial shell positioned between two rigid and parallel planes; that is, tonometer and underlying bone. The undeformed radius of the artery is *r* and the distance between the planes is *2b*.

While hold-down pressure increases, arterial wall is deformed and the distance of planes decreases. And, the total external force and the length of contact can be formulated as a function of the distance *b*. The solution for the end shear force, *V*, and half length of flattened section, *t*, can be written as a function of planes separation, *b*,

$$V(b) = (0.7157/b^2)EI \tag{1}$$

$$t(b) = \frac{\pi}{2}(r - \frac{b}{0.7185}) \tag{2}$$

where E and I represent the Young's modulus and the moment of inertia of the artery, respectively.

If the dimensions and forces acting on the ends of the flattened wall segment are known, the contact stress σ_c can be calculated. When the segment of artery has changed shape from cicular to straight, the flexure equation can ben written as a difference in curvature as equation (3).

$$\frac{1}{r_1} - \frac{1}{r} = \frac{-M}{EI} + \frac{\alpha}{AG}\frac{dV}{dx} \tag{3}$$

where r = initial radius; r_1 = radius after distortion; M = applied bending moment; I = moment of inertia for flattened wall cross-section; α = a geometric constant, 1.5; A= cross-sectional area of flattened wall; G = shear modulus of arterial wall, $E/2(1+\upsilon)$; υ = Poisson's ratio.

Then, considering the balance of shear forces and bending moments in a radial plane of the vessel wall, $dM/dx - V = 0$ is given and let $\beta^2 = AG/\alpha EI$, equation (3) can be modified as

$$\frac{d^2M}{dx^2} - \beta^2 M = -\frac{\beta^2 EI}{r} \tag{4}$$

Then, $M(x)$'s general solution can be expressed,

$$M(x) = C_1 e^{\beta x} + C_2 e^{-\beta x} + \frac{EI}{r} \tag{5}$$

As $V(x)$ can be obtained by the differential of $M(x)$, the constants C_1 and C_2 are dtermined from the shear foce relations,

$$V(x) = C_1 \beta e^{\beta x} - C_2 e^{-\beta x} \tag{6}$$

Considering the contact force per unit length $q(x)$ and substitition $q(x)=dV/dx=0$ with contact stress defined as $\sigma_c(x)=-q(x)/\Delta L$, then, the relationship between contact stress and deformed distance is given,

$$\sigma_c = V(b)\beta \frac{\cosh \beta x}{\sinh \beta t} \tag{7}$$

In Fig. 3, the computed contact stress distribution along the flattened vessel wall is plotted. In this computation, the radial artery is supposed to be isotropic and geometric and material values are summarized below (Westerhof et al., 1969):

E = 8 * 10^6 dynes/cm^2
G = 2.67 * 10^6 dynes/cm^2
υ = 0.5
r = 0.172 cm
h = 0.043 cm.

The computed contact stress, $\sigma_c(x)$ is plotted as function of x and x=0 corresponds to a point directly over the axis of the vessel. Each percentile number of curves represents a ratio of given deflection, y to initial radius, r. From the results, we can gain much insights of the relationships between the degree of deflection and contact stress distribution. In detail, as the degree of deflection increases, the contact length between pressure transducer system and arterial wall increases so to be almost 0.10cm (-0.05~0.05cm) at the deflection of 70%. And, we can also know that, at 30% deflection, the larger deformational stress are needed than that at the other degrees of deflection shown in Fig. 3 and the minimum contact stress under a contact section is in inverse proportion to the degree of deflection.
Consequently, with this mathematical model, not only the operation principle can be explained thoroughly but also it is expected to help set up a proper measuring process and design a reliable sensor system.

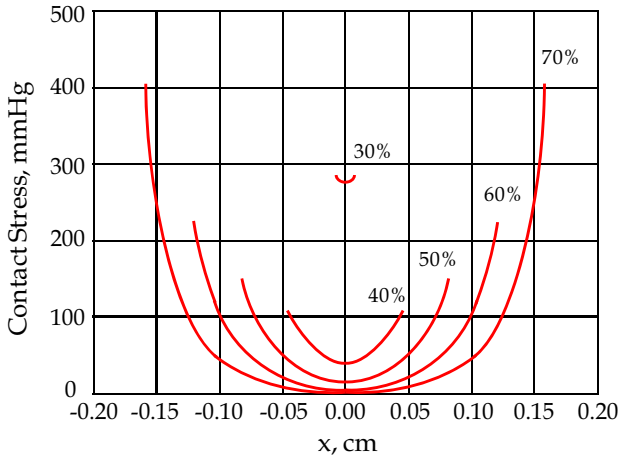

Fig. 3. Computed contact stress distribution for given deflection in the y direction (Drzewiecki et al., 1983)

2.3 Reliable measurement

The arterial tonometry is easy and useful non-invasive measurement technique but is susceptible to wrong measurement. To deal with this problem, the subject's variation caused by physiological and psychological variations, movements, and so on during the measurement should be minimized first and, then, the several conditions mentioned in section 2.1 should be satisfied. An overriding factor, the subject's variation, can be suppressed by following the standardized measurement conditions as listed in Table 1 (Van Bortel et al., 2002). For example, some radial and aortic pulse parameters, such as time to 1st and 2nd peak at radial artery, ejection duration, augmentation index, heart rate etc., were significantly different between upright position and supine position (Nam, 2009).

Confounding factor	In practice
Room temperature	Controlled environment kept at 22±1°C
Rest	At least 10 min in recumbent position
Time of the day	Similar time of the day for repeated measurements
Smoking, eating	Subjects have to refrain, for at least 3h before measurements, particularly from drinking beverages containing caffeine
Alcohol	Refrain from drinking alcohol 10h before measurements
Speaking, sleeping	Subjects may neither speak nor sleep during measurements
Positions	Supine position is preferred. Position (supine, sitting) should be mentioned
White coat effect	Influence on blood pressure and pressure dependent stiffness
Cardiac arrhythmia	Be aware of possible disturbance

Table 1. Recommendations for standardization of subject conditions

A major practical problem is how to make the sensor centered on the artery. Actually, reliable measurements can be obtained only after painstaking adjustment of the sensor location (Kelly et al., 1989). To solve this problem, multi-element sensors, which consist of multi-force transducers and arterial riders at the end of each transducer, have been developed (Terry et al., 1990). The array needs to be positioned with enough precision so that one or more elements of the array are centered over the artery and they can be identified by comparing the measured pressure values at each element. The first step to identify the center positioned element is to examine the measured pulse amplitudes, that is, differences between the maximum and the minimum of a pulse waveform. If an element is precisely centered over the artery, this element will get the largest amplitude. However, it is not sufficient to determine the centered element so that second step is followed. In the second step, the pressure distribution of sensor at a diastolic period is examined.

In Fig. 4, a multi-element tonometer sensor and an underlying and partially compressed artery at the instant of diastole are illustrated. Assuming that the diastolic pressure is 80mmHg, elements 4-6 lying over the flattened artery wall measure the intra-arterial pressure, 80mmHg. However, the pressures of elements 2, 3, 7, and 8 are all significantly greater because the artery wall under these elements is bent to a very small radius and, at the both ends, large bending moments (or contact stresses) are transmitted by the artery wall as shown in Fig. 3 in section 2.2. So, the sensor element corresponding to the local minimum should be determined as the centered element (Drzewiecki et al., 1983).

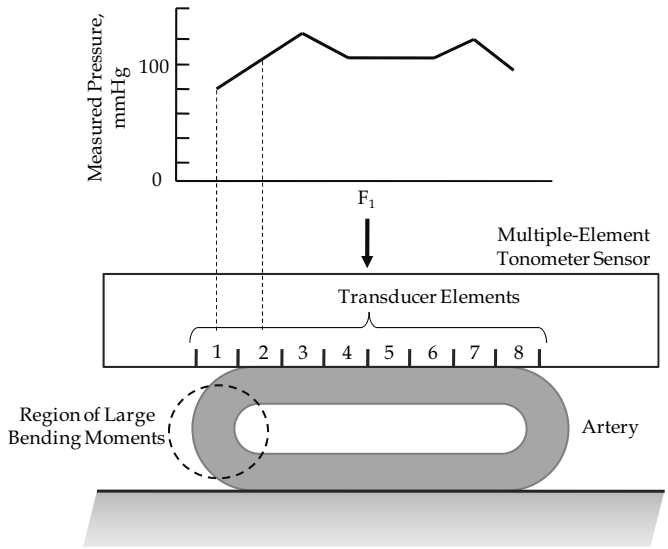

Fig. 4. Bending effect on pressure distribution (Eckerle, 1981)

Determining the centered sensor element is not enough for reliable measurement; the degree of arterial flattening is also important. Arterial flattening depends on the interaction of anatomical factors with the hold-down force, F_1 in Fig. 4. The appropriate hold-down force, which minimizes the contact stress of arterial wall and maximizes the amplitude of pulse pressure, must be determined for each subject before reliable tonometric measurement can be made. An algorithm for automatic identification of the appropriate hold-down pressure was developed (Eckerle et al., 1989). Briefly, the algorithm fits a third order polynomial to the signal recorded while increasing or decreasing hold-down pressure and then determines the timing of the appropriate hold-down pressure from polynomial coefficients.

To determine this hold-down pressure more exactly, we have developed a step motor controlled robot arm including a multi-array sensor on its tip and a laser displacement sensor (LK-G30, Keyence Co., Japan) embedding an algorithm for the elimination of diffused reflection effects which happens on skin inevitably. We lowered the robot arm by increasing the number of motor steps so that the tip of robot arm approaches the skin closely and, then, indented the skin over the radial artery gradually. Therefore we could record the displacement of the robot arm which is roughly related to the degrees of arterial deflection in section 2.2, as well as hold-down pressure and radial pulse waveforms simultaneously. The displacement and approximated degrees of deflection can be used to check whether the determined appropriate hold-down pressure corresponds to the reasonable range of deflection degrees (60%-70%); Assuming the thickness of skin and tissue layer as 3.0 mm, the diameter of radial artery as 3.0 mm and the maximum decrement of skin/tissue layer thickness as 0.5 mm or less, the appropriate hold-down pressure will correspond to 2.3-.2.6 mm displacement from skin contact level approximately. In Fig. 5, an example of robot arm displacement values and corresponding radial pulse waveforms depicted as dimensionless are shown. Since the skin contact seems to occur at around 3.5 mm in y-axis and the pulse pressure can be found to be biggest at near 1 mm in y-axis, the decreased diameter is

presumed to be about 2.5 mm and it falls within the reasonable range of deflection degrees well.

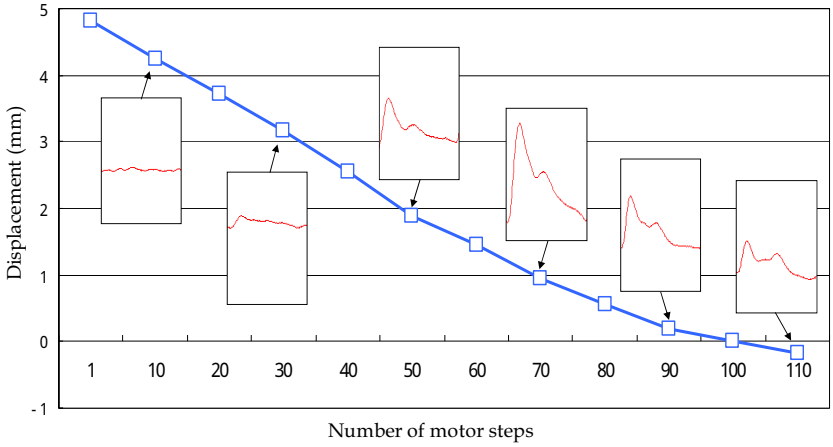

Fig. 5. Displacements of the robot arm and corresponding radial pulse waveforms

Consequently, despite the easiness to be performed, the reliable measurement needs to pay much attention to keep the subject's variation minimized and to have sophisticated strategies to determinate the centered sensor element and the appropriate hold-down pressure.

3. Arterial stiffness estimation

Increased arterial stiffness accelerates the speed at which the left ventricular ejection pressure wave travels through the arteries, and leads to an earlier return of the reflected pressure wave back to the left ventricle. As a result, the reflected pressure wave arrived during systole causes the augmentation of the late systolic pressure (afterload) on the left ventricle. So, the degrees of augmentation can be used as one of the arterial stiffness estimators.

3.1 Augmentation index

The arterial pressure waveform is a composite of the forward pressure wave generated ventricular contraction and a reflected wave. Waves are reflected from the periphery, mainly at branch points or sites of impedance mismatch. In elastic vessels, because PWV is low, reflected wave arrives back at the central arteries earlier, adding to the forward wave and augmenting the systolic pressure. This phenomenon can be quantified through the augmentation index (AIx) – defined as the ratio of the difference between the second and first systolic peaks (P2-P1) to the pulse pressure as shown in Fig. 6. The augmentation index is dimensionless and usually expressed in percentage, but it does not depend on the absolute pressure. While pacing the heartbeat rhythm, AIx was shown to be significantly and inversely related to heart rate ($r = -0.70$, $p < .001$) due to an alteration in the relative

timing of the reflected pressure wave (Wilkinson et al., 2002). So, using the relationship between AIx and heart rate, corrected AIx at 75 bpm (AIx@75) has been commonly used. Even though peak systolic pressures are similar, different augmentation indexes explain that different loading effects arise on the left ventricle. Increased AIx due to arterial stiffening may occur with aging or in disorders such as hypertension, diabetes or hypercholesterolemia. And, because the augmentation means the increase of afterload in systolic period and the eduction of coronary artery perfusion pressure and leads to greater risk of angina, heart attack, stroke and heart failure, it is quite useful clinically.

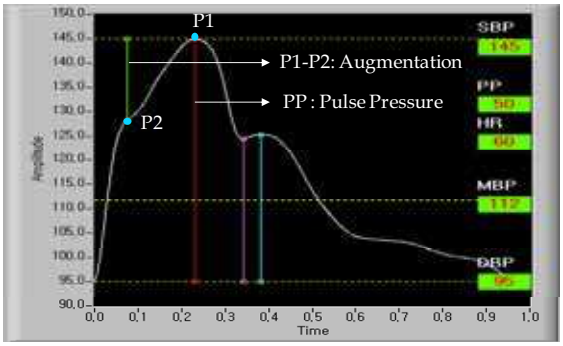

Fig. 6. An example of aortic pulse pressure waveform and augmented pressure

3.2 Transfer function

Aortic pressure waveform for AIx calculation can be estimated either from the radial artery waveform, using a transfer function, or from the common carotid waveform.

And, a transfer function between aortic pressure radial pressure signals can be derived by the linear ARX model. The ARX linear model describes the properties of a system on the basis of its immediate past input and output data as

$$T(t)=-a_1T(t-1)-a_2T(t-2)-...-a_m(t-m) \\ +b_1P(t-1)+...+b_nP(t-n) \tag{8}$$

where T(t) and T(t-i) [i=1, 2, ..., m] are present and previous output (radial tonometer), respectively, and P(t-i) are previous input (aortic pressure). The a's and b's are the parameters of the model, and m and n represent the order of the model, that is, the number of previous input-output values used to describe the present output. This methodology yields more statistically stable and thus reliable spectral estimates from limited data compared with nonparametric approaches, for example, a Fourier transform.

The transfer function is estimated with the aortic pressure used as input and the radial tonometer signal as output. An inverse TF derived from TF can be used to reconstruct the aortic pressure from the radial pulse as follows:

$$P(t-1)=-b_2/b_1P(t-2)-...-b_n/b_1P(t-n) \\ +1/b_1T(t)+a_1/b_1T(t-1)+...+a_m/b_1T(t-m) \tag{9}$$

In general, the model order for TF estimate is selected as 10, that is, 10 'a' coefficients and 10 'b' coefficients are used. Meanwhile, a critical problem lies on this approach. The low gain of the TF in the frequency range above 8 to 10 Hz brings out the high gains of the inverse TF so that it amplifies high-frequency noise and distorts the reconstructed aortic pressure waveform. This problem can be solved by convolving the inverse TF with a low-pass filter having a cut-off frequency at which the magnitude of the TF gain function declines below 1. While the mean TF of an individual at several steady-states is called as an individual transfer function (ITF), a global transfer function (GTF) are obtained by averaging the ITF from all participated patients. Chen et al. have reported that TFs varied among patients; coefficient of variation was 24.9% for peak amplitude and was 16.9% for frequency at peak amplitude, respectively. Despite this, the GTF estimated central arterial pressure to ≤0.2±3.8mmHg error, arterial compliance to 6±7% accuracy, and augmentation index to within -7% points (30±45%) (Chen et al., 1997). In addition, because the radial blood pressure is higher than the brachial blood pressure, brachial artery pressure is used as surrogate of radial artery pressure for the calibration of central pressure.

3.3 Augmentation point detection algorithm

As an augmentation pressure is a determinate factor in AIx calculation, a reliable AIx estimation depends on accurate detection of augmentation point mostly. Even if one can indicate the timing of the augmentation point easily such a local minimum in the first derivative that was in the range from 0 to 50 msec of the peak flow (Chen et al., 1996), it is hard to detect an exact augmentation point. In late 80's, utilizing a non-invasively measured flow velocity signal, an earnest algorithm which could detect an augmentation point of ascending aortic pressure was developed (Kelly et al., 1989). Kelly et al. showed that the first zero-crossing of the fourth derivative corresponded to the beginning of the pressure wave upstroke and the second zero crossing in the same direction corresponded to the shoulder, that is, the augmentation points. And, they also found a good correlation between the time to the second zero crossing of the fourth derivative (x) and the timing of the peak of flow (y), which was the time-delayed sign to arrival of reflected wave; $y=0.91+1.31x$, $R=0.75$. So, it was suggested that an augmentation points could be determined as the second zero crossing of the fourth derivative as shown in Fig. 7. Recently, a detection method with only carotid pulse pressure was proposed (Gatzka et al., 2001). In this study, the augmentation point was defined as the first zero crossing from positive to negative of the fourth derivative and occurs 55 msec after the onset of systole pressure.

However, these mentioned studies do not fit well to all types of aortic pressure waveform; the aortic pressure waveform can be divided into three broad categories generally (Murgo et al., 1980). Particularly, a subject-sensitive searching interval for the detection of augmentation point should be fixed empirically so to lack in flexibility.

So, our colleague suggested a syntactic algorithm in which they tried first to indicate an augmentation point on the first derivative with a searching condition, if failed, then, on the second derivative with another searching condition, if failed again, lastly on the third derivative with the other searching condition within a first searching range from the first peak to second negative slope zero crossing of the first derivative (Im & Jeon, 2008). Nevertheless, if no augmentation point were detected, they considered the augmentation point located after the systolic peak of aortic pulse not before the systolic peak. Then, within a second searching range from the first negative slope zero crossing to the second positive

slope zero crossing of the first derivative, they tried to detect an augmentation point with similar strategy mentioned above. Finally, they reported that the percentage error in AIx was 4.82± 16.9, smaller than 39.5± 39.4 reported by Fetics et al. (Fetics et al., 1999) and smaller than 27± 22 reported by Chen et al. (Chen et al., 1997).

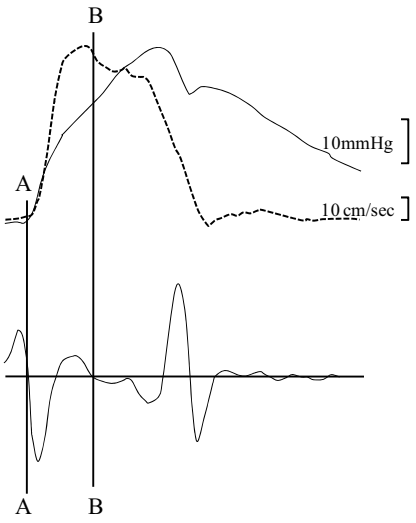

Fig. 7. An example of ascending aortic pressure form(solid line above), blood flow (dashed line above) and corresponding fourth derivative of pressure waveform(solid line below) (Kelly et al., 1989)

4. Emerging issues

Although the radial areterial tonometry has been widely used to estimate the arterial function, there remains many research issues to be studied. For examples, the geometric and hemodynamic characteristics of radial artery and the effects of measuring position selection on AIx have not be studied thoroughly. One the other hand, there is criticism for the use of transfer function. So, in the following sections, we want to deal with the radial artery characteristics and the importance of measuring position. And, we will introduce the latest attempts to estimate the arterial stiffness with radial pulse waveform itself and to apply the radial tonometry to the oriental pulse diagnosis.

4.1 Geometric and hemodynamic characteristics of radial artery

In oriental medicine, before at least about 2,000 years, it has been asserted that the pulse pressures, the optimal hold-down pressures for pulse diagnosis and even the pulse images are different among adjacent three diagnosis positions over the radial artery. So, we performed an experiment of ultrasonography on radial artery to examine the geometrical and hemodynamic characteristics in 2007. The six measuring positions on each hand were selected as shown in Fig. 8. The distal three positions were the well-known oriental pulse diagnosis positions and the other proximal three positions were non-pulse diagnosis

positions which were located at regular intervals. The intervals between adjacent positions ranged from 1.20cm to 1.45cm and it was determined as to be proportional to the length of elbow individually by a skillful oriental medical doctor.

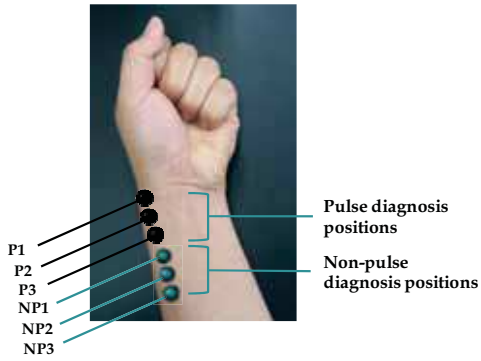

Fig. 8. An example of selected measuring positions composed of three pulse diagnosis positions and three non-pulse diagnosis positions

Under the approval of the Institutional Review Board of the Oriental Medicine Hospital at Daejeon University, South Korea, 44 healthy male and female in their 20s were participated as subjects. The geomtrical parameters, the depth and diameter of radial artery, and the hemodynamic parameters, the maximum and average blood velocities, were measured three times in random order at 12 positions, that is, each 6 positions in left and right sides. These positions are marked with tiny metal wires so to be recognized in an ultrasound image. In this experiment, a medical ultrasonography equipment (Volusion 730 Pro, GE Medical, USA) was utilized to measure the geometrical parameter values in B-Mode and the hemodynamic parameter values in PW Doppler mode. In the geometrical measurement, because the geometrical parameters varied dynamically during a heartbeat, the geometrical parameters were obtained only from the B mode images frozen at diastolic periods. The timing of diastolic period was determined with simultaneously measured photo-plethysmogram (PPG) from the index finger of each subject.

The measured values of parameters at 12 positions are summarized in Table 2 and reported as mean±SD. And, the variation tendency of all parameters from P1 to NP3 is also shown with mean values in Fig. 9. One-way ANOVA was conducted to examine whether the depths, the diameters and the blood flow velocities among 6 positions were different for each hand. A p-value<0.05 was considered statistically significant. As a result, the vessel depths($p < .001$), vessels diameter ($p < .001$) and average flow velocities($p < .001$) among 6 positions, that is, P1, P2, P3, NP1, NP2 and NP3 were showed to be significantly different in each hand. And, when those parameters of left and right hand were compared, the vessel depths of P1, NP2 and NP3, the vessel diameter of P3 and the average flow velocity of all 6 positions were found to be also different signifcantly between left and right hand. In details, as for the vessel depths, those among P1, P2 and P3 differed significantly (left: $p = 0.001$; right: $p < .0001$), but no significant differences were observed among non-pulse dianosing positions. Contrarily, when the vessel diameter was evaluated, no significant differences

were observed among P1, P2 and P3. However, there was a statistically significant difference among NP1, NP2, and NP3 (left: p = 0.0002; right: p = 0.0032).
Consequently, in further studies on radial pulse wave, 1) the geometrical difference between the pulse diagnosis positions and the non pulse diagnosis positions, and even among P1, P2 and P3 and 2) the hemodynamic radical change near the periphery must be considered.

Parameters		P1	P2	P3	NP1	NP2	NP3
Left	Vessel depth (mm)	3.26± (0.71)	2.74 ± (0.66)	3.32 ± (0.85)	3.79 ± (1.09)	3.90± (1.11)	4.17 ± (1.26)
	Vessel diameter (mm)	2.52 ± (0.36)	2.42 ± (0.35)	2.52 ± (0.30)	2.54 ± (0.32)	2.51 ± (0.31)	2.51 ± (0.31)
	Maximum blood flow velocity (cm/sec)	41.68 ± (12.39)	55.34 ± (14.70)	56.26 ± (11.82)	54.98 ± (12.23)	56.36± (12.21)	57.66 ± (13.57)
	Average blood flow velocity (cm/sec)	5.75± (3.25)	9.24 ± (4.86)	9.51 ± (4.44)	9.81 ± (5.24)	9.66 ± (4.51)	10.14 ± (5.04)
Right	Vessel depth (mm)	3.60± (0.82)	2.74 ± (0.72)	3.36± (1.14)	3.95± (1.36)	4.32 ± (1.42)	4.64 ± (1.41)
	Vessel diameter (mm)	2.47 ± (0.39)	2.37 ± (0.32)	2.46 ± (0.33)	2.53 ± (0.41)	2.55 ± (0.34)	2.55 ± (0.33)
	Maximum blood flow velocity (cm/sec)	35.50± (4.64)	49.28 ± (11.95)	50.91 ± (11.55)	51.43± (12.53)	52.85± (13.15)	53.94 ± (12.13)
	Average blood flow velocity (cm/sec)	4.64 ± (2.99)	7.46 ± (4.24)	7.98± (4.41)	8.26± (4.44)	8.45 ± (5.12)	8.39 ± (4.43)

Table 2. Summarized measurement results: the depth, the diameter of radial artery, and the blood blow velocity at 12 positions

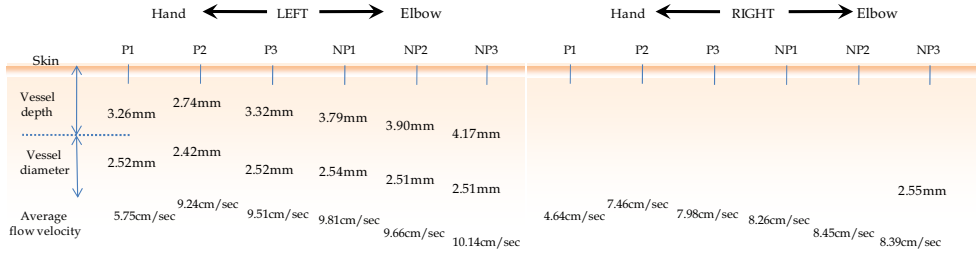

Fig. 9. The variation of parameters along the 6 positions composed of three pulse diagnosis positions and three non-pulse diagnosis positions in both hands

4.2 Measuring position effects on AIx

As referred in section 4.1, the geometric and hemodynamic characteristics are different among pulse diagnosis positions. So, we examined the measuring position effects on AIx.
In this study, 20 young male persons were involved, who had no cardiovascular disease history and were in twenties, normotensive and within the normal range (18.5~24.9 kg/m^2) of the body mass index (BMI). And, using the SphygmoCor apparatus (AtCor Medical, Australia), we measured twice the baseline and the signal strength, which correspond to the hold-down pressure and the measured pulse pressure, respectively, and the AIx@75 at the

P1, P2, and P3 of left hand. To avoid any bias in data collection, we randomized the order of measuring positions for each subject. Especially, to obtain the noise minimized and high intensity signals, the signal strength, which represents the difference between the maximum and the minimum of the pulse waveform, were kept over 360 and the variation of signal strength and baseline were monitored to be within ±100, ±200, respectively. If these were not contented, the measurement of radial pulse waveform was designed to be performed again. Furthermore, the signals, of which the OI (operator index) provided by the SphygmoCor software were over 90 and the sub-parameters of OI, that is, average pulse height, pulse height variation, diastolic variation, shape deviation, and maximum dP/dT fell in agreeable green range, were only selected for the statistical analysis. First, we tested the repeatability of measurement with two-way repeated measures ANOVA, by which the differences in the average of baseline, pulse strength, and AIx@75 between first and second measurement for each position were examined.

As a result, we could not find any difference at 5% of statistical significance level so that the measurement process was showed to be well-controlled. In detail, the mean and the standard error (mean±SEM) of the differences between AIx@75s of the two repeated measures were estimated respectively as -0.45±0.63, 0.05±0.72, and -0.15±0.68 at P1, P2, and P3. Then, we tested the differences of baseline, pulse strength, and AIx@75 among P1, P2 and P3 with two-way repeated measures ANOVA analysis. In Table 3, the measured values (mean±SD) of three parameters at each positions and p-values calculated by the two-way repeated measures ANOVA are summarized. Finally, in all parameters including AIx@75, significant differences among P1, P2 and P3 were found. From this, we could conclude that careless selection of measuring position might bring out different or wrong estimation of augmentation index. Interestingly, no significant difference was found in the radial waveform parameters including radial AIxs among P1, P2 and P3.

	P1	P2	P3	*p*-value
Baseline	1108.8±273.6	962.5±170.9	1033.8±246.4	4.625E-4
Signal strength	511.5±78.0	543.1±82.6	472.6±69.5	2.354E-8
AIx@75	-0.23±5.56	-1.83±5.97	-2.28±5.73	0.004

Table 3. Differences of baseline, signal strength and AIx@75 among P1, P2 an dP3

We also analyzed the difference of AIx among P1, P2 and P3 using a well-known multiple comparison analysis, Duncan test, and the results are shown in Table 4. It probably seemed to be correlated with the fact that the blood flow velocity at P1 was quite different from that of P2 and P3 as described in section 4.1. Consequently, we want to suggest that it is necessary to establish a more detailed guideline for the selection of measuring positions so to minimize the mistakes in treatment based on the AIx.

	P1	P2	P3
Mean	-0.225	-1.825	-2.275
SD	5.558	5.597	5.729
F	5.867		
p-value	0.004		
Group	A	B	B

Table 4. Multiple comparisons on AIx@75

4.3 Stiffness estimation without a transfer function

The transfer function has been widely used to reconstruct the aortic pressure waveform from the measured radial waveform. However, the reliability of this is still controversial. Although the use of a general transfer function has been well established and has demonstrated its reliability for calculating central PP (Williams et al., 2006), the accuracy of this method for the calculation of aortic AIx has been disputed (Millasseau et al., 2003). Indeed, even though the general transfer function has been reported to provide accurate estimates of central PP, compliance, and other low-frequency component features of the central waveform, it has been urged to be less accurate and to induce greater between-subject variability at high frequency components which contributes to determine the augmentation index (Segers et al., 2005). So, an alternative and direct approach without a transfer function has been needed. In a recent study, the reliability of carotid AIx estimation from nontransformed radial AIx has been shown (Melenovsky et al., 2007). The major results can be summarized are below:

- Carotid AIx significantly correlated with radial AIx independent of age, mean BP, gender and body mass index. This correlation was significant under baseline conditions, during a cold-pressor test, and after sublingual administration of nitroglycerine.
- The changes in radial AIx and carotid AIx caused by provocative maneuver were also significantly correlated.
- The non-linear correlation between radial (or carotid) AIx and late systolic pressure-time integral, defined as afterload was found.

If more cases of radial AIx's or a third index's compatibility to the aortic AIx in the treatment of hypertension are accumulated, the AIx estimation method with a transfer function might be disused spontaneously.

4.4 Applications in the oriental medicine

In oriental medicine, the radial arterial pulse has been widely believed as a reflection of health condition for over at least two thousand years. However, the pulse diagnosis, which is similar to the radial artery tonometry but more complex, has been criticized as having some ambiguities and a susceptibility to being subjectified because almost procedure have been quite dependent on the subjective and not-exchangeable feeling of oriental medical doctors (OMDs).

A patient's pulse diagnosis has been determined with one or more of the 28 types of so-called pulse image defined as pulsation pressure distributions on the 3 pulse diagnosis positions while varying hold-down pressure. All verbal descriptions related with the 28 types of pulse image could be divided into the readily measurable physical components, that is, the depth, the frequency, the strength, the width, and the length of pulsation, and the others (Ryu et al., 2007). With these 5 components, 10 types of pulse images are able to diagnosed: that is, floating and sinking pulses, slow pulse and fast pulses, forceful and deficient pulses, large and fine pulses, and long and short pulses. To measure these quantities reliably, our colleagues in KIOM (Korea Institute of Oriental Medicine) have tried to develop a few types of pulse diagnosis devices based on 3 or 5 degrees of freedom robot arms embedding a multi-array pressure sensor on its tip since 2006 (Lee, 2007). The multi-

array sensor can measure the hold-down pressure and the pulsation pressure distribution simultaneously at 10 different hold-down pressures ranged from 0 to 500g·f. From these obtained signals, we can extract some useful information for the pulse diagnosis such as the profile of pulse pressure vs. hold-down pressure, the maximum pulse pressure at a certain hold-down pressure defined as an optimal hold-down pressure, the pulsation frequency, the pressure distribution under the array sensor at the optimal hold-down pressure etc.
On the other hand, we have obtained over 4,000 volunteer's data with one of these systems and have also collected their clinical information including blood pressures, body temperatures, health questionnaires, and quantitative pulse diagnosis records by 3 OMDs. In these pulse diagnosis records by OMD, the membership degrees to 10 pulse images each have been included. With this database, we are examining the normal and abnormal range of each quantity and the interactions between each quantity, and each quantity's contributions to diagnosis into 10 types of pulse images and we are developing some pulse diagnosis discriminant functions (Lee et al., 2007).
For now, the floating and sinking pulses might be correlated to the blood pressure - systolic pressure($r=0.405$, $p<0.005$) and diastolic pressure($r=0.398$, $p<0.005$). And, between the pulse waveforms of the forceful and deficient pulses, significant differences has been shown in the maximum pulse pressure ($p=0.000$) and the systolic pulse width ($p=0.000$). No doubt, the slow and fast pulses are highly correlated to the heart rate. The wide and fine pulse are inferred to be related to the contact length described in section 2.2 so that they should be examined on its correlation with the blood vessel's diameter directly, the elasticity of blood vessel, or E involved in equation (7) as a factor of β. Lastly, the long and short pulses are guessed to be related with the effective systolic time and systolic volume.
In further studies, we hope to reveal the underlying physiological factors of these pulse images and to examine the relationship between these pulse images and clinical symptoms mentioned in oriental medicine literatures. In that case, with radial arterial tonometry, we can provide unheard of healthcare contents originated from the oriental medicine.

5. Conclusion

In this chapter, we presented the one of most attractive arterial stiffness estimation method with AIx calculated from radial pulse waveform measured by radial arterial tonometry.
In the first part, we tried to enhance the understanding of arterial tonometry by explaining the operation principle and continuous mathematical model of the relationship between arterial wall deformation and contact stress. We also dealt with three causes of measurement errors; subject's variation, uncertainty of sensor location and non-appropriate hold-down pressure. Concerning these, we summarized factors affect subject's variation and introduced some algorithms of searching the centered sensor element and of determining the optimal hold-down pressure for reliable measurement.
In the middle part, the estimation method of arterial stiffness with AIx was elucidated. In details, the clinical importance of AIx was explained and some ways to generate an aortic pressure waveform with transfer function and to detect an augmentation point for calculating AIx were surveyed.
In the latter part, some emerging issues on radial tonometry were provided. First two were about the geometric and hemodynamic characteristics of radial artery and the effect of measuring position on AIx ignored comparatively heretofore. Next one was about recent

attempts to estimate arterial stiffness with radial AIx extracted from radial pulse waveform itself. In last, we exclusively reported the development of robot arm adopting the radial tonometry for oriental pulse diagnosis in Korea, and the possibility of offering new healthcare contents with this system.

Though further studies, we expect, all underlying principles are revealed and all conditions for reliable measurement are established and made controllable. And, we hope that more concrete clinical evidences are accumulated and potential applications are established so that arterial tonometry would be used usefully and frequently as much as electrocardiography does.

6. References

Chen, C. H.; Ting, C. T.; Nussbacher, A.; Nevo, E.; Kass, D. A.; Pak, P.; Wang, S. P.; Chang, M. S. & Yin, F. C. P. (1996). Validation of carotid artery tonometry as a means of estimating augmentation index of ascending aortic pressure. *Hypertension*, Vol. 27, pp. 168-175

Chen, C.; Nevo, E.; Fetics, B.; Pak, P. H.; Yin, F. C. P.; Maughan, W. L. & Kass. D. A. (1997). Estimation of central aortic pressure waveform by mathematical transformation of radial tonometry pressure. *Circulation*, Vol. 95, pp. 1827-1836

Darne, B.; Girerd, X.; Safar, M.; Cambien, F. & Guise, L. (1989). Pulsatile versus steady component of blood pressure : a cross-sectional analysis and a prospective analysis on cardiovascular mortality. *Hypertension,* Vol. 13, pp. 392-400

Drzewieki, G. M.; Melbin, J. & Noordergraff, A. (1983). Arterial tonometry : Review and anlysis. *J. Biomechanics,* Vol. 16, No. 2, pp. 141-152

Eckerle, J. S. (1981). Noninvasive blood pressure monitoring transducer. *US Patent* 4,269,193

Eckerle, J. S. (1989). Blood pressure monitoring method and apparatus. *US Patent* 4,799,491

Eckerle, J. S. (2006). Tonometry, Arterial, In: *Encyclopedia of Medical Devices and Instrumentation*, Webster, J. G., 2nd Edition, 402-409, Wiley, ISBN: 978-0-471-26358-6

Fetics, B.; Nevo, E.; Chen, C. H. & Kass, D. A. (1999). Parametric model derivation of transfer function for noninvasive estimation of aortic pressure by radial tonometry. *IEEE Transcations on Biomdeical Engineering*, Vol. 46, pp. 698-706

Gatzka, C. D.; Cameron, J. D.; Dart, A. M.; Berry, K. L.; Kingwell, B. A.; Dewar, E. M.; Reid, C. M. & Jennings, G. L. R. (2001). Correction of carotid augmentation index for heart rate in elderly essential hypertensives. *Am J Hypertens*, Vol. 14, pp. 573–577

Gerard, M. & Alain, P. G. (1999). Influence of arterial pulse and reflective waves on blood pressure and cardiac function. *American Heart Journal,* Vol. 138, No. 3, pp. S220-S224

Im, J. J. & Jeon, Y. J. (2008). Estimation of the central aortic pulse using transfer function and improvement of an augmentation point detection algorithm, *Korean Journal of Electronics Engineering*, Vol. 45, No. 3, pp. 68-79 (*in Korean*)

Kelly, R.; Hayward, C.; Avolio, A. & O'Rourke, M. (1989). Noninvasive determination of age-related changes in the human arterial pulse. *Circulation*, Vol. 80, pp. 1652-1659

Lee, J. (2007). Traditional Medicine Instrument in Korea - Development States of Pulse Analyzer, *7th Annual Meeting for Japanese Society of Integrative Medicine*, pp. 50, Ichinobo hotel, Dec. 2007, Matsushima, Japan

Lee, Y. J.; Lee, J.; Jang, E. S.; Choi, E. J.; Lee, H. J. & Kim, J. Y. (2007). A study of floating and sink pulse diagnosis : analysing of pulse wave parameter and typical pulse pattern, *ICMART2007,* pp. 14-17, ISBN, Hotel Fira Palace, Jun. 2007, Barcelona, Spain

Melenovsky, V.; Borlaug, B. A.; Fetics, B.; Kesseler, K.; Shively, L. & Hass, D. A. (2007). Estimation of central pressure augmentation using automated radial artery tonometry. *J Hypertens*, Vol. 25, pp. 1403-1409

Millasseau, S. C.; Patel, S. J.; Redwood, S. R.; Ritter, J. M. & Chowienczyk, P. J. (2003). Pressure wave reflection assessed for the peripheral pulse. Is a transfer function necessary? *Hypertension,* Vol. 41, pp. 1016-1020

Murgo, J. P.; Westerhof, N.; Giolma, J. P. & Altobelli, S. A. (1980). Aortic input impedance in normal man: relationship to pressure wave forms. *Circulation*, Vol. 62, No. 1, pp. 105-116

Nam, K.C.; Kim E.G.; Heo, H.; Huh, Y. (2009). Effect of Subject Posture on Pulse Wave Measurement, *The 24th International Technical Conference on Circuits/Systems, Computers and Communications (ITC-CSCC 2009),* pp. 499-501, Jeju KAL Hotel, Jul. 2009, Jeju, Korea

Pressman, G. & Newgard, P. (1963). A transducer for the continuous external measurement of arterial blood pressure. *IEEE Trans. Bio-Med. Electron.,* Vol. BME-10, pp. 73-80

Roman, M. J.; Devereux, R. B.; Kizer, J. R.; Lee, E. T.; Galloway, J. M.; Ali, T.; Umans, J. G. & Howard, B. V. (2007). Central pressure more strongly relates to vascular disease and outcome than does brachial pressure. *Hypertension*, Vol. 50, pp. 197-203

Ryu, H. H.; Lee, S. W.; Lee, J.; Lee, Y. J. & Kim, J. Y. (2007). The Literary Study on the Physical Quantification of Pulse Types. *Korean J. Oriental Physiology & Pathology*, Vol. 21, No. 6, pp. 1381-1387 (*in Korean*)

Segers, P.; Rietzschel, E.; Heireman, S.; Du Buyzere, M.; Gilbert, T.; Verdonk, P. & Van Bortel, L. (2005). Carotid tonometry versus synthesized aorta pressure waves for the estimation of central systolic blood pressure and augmentation index. *Am J Hypertens*, Vol. 18, pp. 1168-1173

Terry, S.; Eckerle, J. S.; Kornbluh, R. D.; Low, T. & Ablow, C. M. (1990). Silicon pressure transducer arrays for blood-pressure measurement. *Sensors and Actuators*, Vol. A21-A23, pp. 1070-1079

Van Bortel, L. M; Duprez, D.; Starmans-Kool, M. J.; Safar, M. E.; Giannattasio, C.; Cockfroft, J.; Kaiser, D. R. & Thuillez, C. (2002). Applications of arterial stiffness, Task Force III: recommendations for user procedures. *Am J Hypertens*, Vol. 15, pp. 445-452

Wilkinson, I. B.; Mohammad, N. H.; Tyrrell, S.; Hall, I. R.; Webb, D. J.; Paul, V. E.; Levy, T. & Cockcroft, J. R. (2002). Heart rate dependency of pulse pressure amplification and arterial stiffness. *Am J Hypertens*, Vol. 15, No. 1, pp. 24-30

Williams, B.; Lacy, P. S.; Thom, S. M.; Cruickshank, K.; Stanton, A. & Collier, D. (2006). Differential impact of blood pressure-lowering drugs on central aortic pressure and clinical outcomes: principal results of the Conduit Artery Function Evaluation (CAFE) study. *Circulation,* Vol. 113, pp. 1213-1225

Biomedical Engineering

Edited by Carlos Alexandre Barros de Mello

ISBN 978-953-307-013-1
Hard cover, 658 pages
Publisher InTech
Published online 01, October, 2009
Published in print edition October, 2009

Biomedical Engineering can be seen as a mix of Medicine, Engineering and Science. In fact, this is a natural connection, as the most complicated engineering masterpiece is the human body. And it is exactly to help our “body machine” that Biomedical Engineering has its niche. This book brings the state-of-the-art of some of the most important current research related to Biomedical Engineering. I am very honored to be editing such a valuable book, which has contributions of a selected group of researchers describing the best of their work. Through its 36 chapters, the reader will have access to works related to ECG, image processing, sensors, artificial intelligence, and several other exciting fields.

How to reference

In order to correctly reference this scholarly work, feel free to copy and paste the following:

Jeon Lee and Ki Chang Nam (2009). Tonometric Vascular Function Assessment, Biomedical Engineering, Carlos Alexandre Barros de Mello (Ed.), ISBN: 978-953-307-013-1, InTech, Available from: http://www.intechopen.com/books/biomedical-engineering/tonometric-vascular-function-assessment

INTECH
open science | open minds

InTech Europe
University Campus STeP Ri
Slavka Krautzeka 83/A
51000 Rijeka, Croatia
Phone: +385 (51) 770 447
Fax: +385 (51) 686 166
www.intechopen.com

InTech China
Unit 405, Office Block, Hotel Equatorial Shanghai
No.65, Yan An Road (West), Shanghai, 200040, China
中国上海市延安西路65号上海国际贵都大饭店办公楼405单元
Phone: +86-21-62489820
Fax: +86-21-62489821